# 1

# Fundamentals of Ferroelectric Materials

*Ling B. Kong*[1, 2], *Haitao Huang*[3], *and Sean Li*[4]

[1] *Shenzhen Technology University, College of New Materials and New Energies, 3002 Lantian Road, Shenzhen, Guangdong 518118, PR China*
[2] *Nanyang Technological University, School of Materials Science and Engineering, 50 Nanyang Avenue, Singapore 639798, Singapore*
[3] *Hong Kong Polytechnic University, Department of Applied Physics, 11 Yuk Choi Road, Hung Hom, Kowloon, Hong Kong*
[4] *The University of New South Wales, School of Materials Science and Engineering, High Street, Kensington, Sydney, NSW 2052, Australia*



## 1.1 Introduction

Ferroelectricity is defined as the property of a material, with two characteristics, i.e. (i) spontaneous polarization is present and (ii) it is reversible when subjected to external electric fields [1]. The property was first observed in Rochelle salt and is named so because of its analogy to ferromagnetism, which is a magnetic property of a material that has a permanent magnetic moment [2, 3]. Other similarities include hysteresis loop, Curie temperature ($T_C$), domains, and so on. The prefix, *ferro*, meaning iron (Fe), was used at that time because of the presence of the element in the magnetic materials. However, ferroelectricity has nothing to do with Fe. Even though some ferroelectric materials contain Fe, it is not the originating factor.

Generally, as a material is polarized by an external electric field, the induced polarization ($P$) is linearly proportional to the magnitude of the applied external electric field ($E$), which is known as dielectric polarization. Above the Curie temperature $T_C$, ferroelectric materials are at a paraelectric state. In this case, a nonlinear polarization is present versus an external electric field. As a result, electric permittivity, according to the slope of the polarization curve, is not a constant. At the ferroelectric state, besides the nonlinearity, a spontaneous nonzero polarization was present, as the applied field ($E$) is zero. Because the spontaneous polarization can be reversed by a sufficiently strong electric field, it is dependent on the currently applied electric field and the history as well, thus leading to the presence of the hysteresis loop.

The electric dipoles in a ferroelectric material are coupled to the crystal lattice of the material, so that the variation in lattice could change the strength of the dipoles, i.e. the strength of the spontaneous polarization. The change in the spontaneous polarization, in turn, leads to a change in the surface charge, which causes

*Ferroelectric Materials for Energy Applications*, First Edition.
Edited by Haitao Huang and James F. Scott.

current flow when a ferroelectric material is made into a capacitor without the application of an external field across it. There are two stimuli that can be used to change the lattice structure of a ferroelectric material, i.e. (i) mechanical force and (ii) temperature. The generation of surface charge as a result of the application of an external stress is known as piezoelectricity, while the change in spontaneous polarization in response to the change in temperature is named as pyroelectricity.

To understand ferroelectricity, it is necessary to link with piezoelectricity and pyroelectricity, because they have interesting interrelationships in terms of crystal structures. All crystals can be categorized into 32 different classes. In the theory of point groups, these classes are determined by using several symmetry elements: (i) center of symmetry, (ii) axis of rotation, (iii) mirror planes, and (iv) several combinations of them. The 32 point groups are subdivisions of seven basic crystal systems that are, in order of ascending symmetry, triclinic, monoclinic, orthorhombic, tetragonal, rhombohedral (trigonal), hexagonal, and cubic. Out of the 32 point groups 21 classes are non-centrosymmetric, which is a necessary condition for piezoelectricity to exist. Twenty of them are piezoelectric.

Among the 20 piezoelectric crystal classes, 10 crystals have pyroelectric properties. Within a given temperature range, this group of materials is permanently polarized. Compared to the general piezoelectric polarization produced under stress, pyroelectric polarization develops spontaneously and remains as permanent dipoles in the structure. Because this polarization varies with temperature, the response is named as pyroelectricity. Within the pyroelectric group, there is a subgroup that has spontaneous polarization, which is the ferroelectric materials. On one hand, the polarization in a ferroelectric material is similar to that in a pyroelectric one. On the other hand, these two polarizations are different, because ferroelectric polarization is reversible by an external applied electric field. Therefore, ferroelectricity is defined as the presence of spontaneous polarization that is reversible by an external electric field [4, 5]. Figure 1.1 summarizes the interrelationship among piezoelectric, pyroelectric, and ferroelectric materials, together with general dielectrics. This relationship

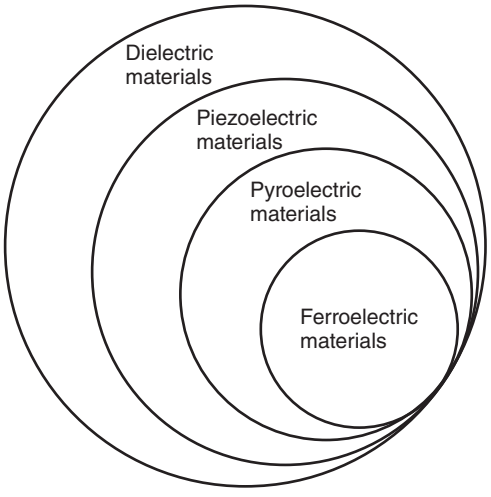


**Figure 1.1** Interrelationship among piezoelectric, ferroelectric, pyroelectric, and dielectric materials. Ferroelectric materials have superior pyroelectric, piezoelectric, and dielectric properties than non-ferroelectric materials.

implies that ferroelectric materials have the highest piezoelectric performance compared to non-ferroelectric materials.

According to Ginzburg–Landau theory, the free energy of a ferroelectric material, without the application of an external electric field and stress, can be expressed as a Taylor expansion in terms of the order parameter, polarization ($P$) [6]. When a sixth order expansion is used, i.e. the eighth order and higher terms are neglected, the free energy is given by

$$\begin{aligned}\Delta G = {} & \frac{1}{2}\alpha_0\left(T - T_0\right)\left(P_x^2 + P_y^2 + P_z^2\right) + \frac{1}{4}\alpha_{11}\left(P_x^4 + P_y^4 + P_z^4\right) \\ & + \frac{1}{2}\alpha_{12}\left(P_x^2P_y^2 + P_y^2P_z^2 + P_z^2P_x^2\right) + \frac{1}{6}\alpha_{111}\left(P_x^6 + P_y^6 + P_z^6\right) \\ & + \frac{1}{2}\alpha_{112}\left[P_x^4\left(P_y^2 + P_z^2\right) + P_y^4\left(P_x^2 + P_z^2\right) + P_z^4\left(P_x^2 + P_y^2\right)\right] + \frac{1}{2}\alpha_{123}P_x^2P_y^2P_z^2\end{aligned} \tag{1.1}$$

where $P_x$, $P_y$, and $P_z$ are the components of the polarization vector in the $x$, $y$, and $z$ directions, respectively, while $\alpha_i$, $\alpha_{ij}$, $\alpha_{ijk}$ are the coefficients that are related to the symmetry of the crystals. These coefficients could be either obtained through experimental measurement or derived from *ab initio* calculation. Generally, in ferroelectric materials, both $\alpha_0$ and $\alpha_{111}$ are positive. For ferroelectrics with a first-order phase transition, $\alpha_{11} < 0$, while for those having a second-order phase transition, $\alpha_{11} > 0$.

During the phase transition from cubic to tetragonal phase, the spontaneous polarization, $P_s$, of a ferroelectric can be derived in a relatively simple way, if the free energy is described as a 1D expression, which is given by

$$\Delta G = \frac{1}{2}\alpha_0\left(T - T_0\right)P_x^2 + \frac{1}{4}\alpha_{11}P_x^4 + \frac{1}{6}\alpha_{111}P_x^6 \tag{1.2}$$

The solution of the free energy is characterized with a shape that has a double well potential, with two free energy minima at $P = \pm P_s$, where $P_s$ is the spontaneous polarization. At these two minima, the derivative of the free energy is zero, i.e.

$$\frac{\partial(\Delta G)}{\partial P_x} = \alpha_0\left(T - T_0\right)P_x + \alpha_{11}P_x^3 + \alpha_{111}P_x^5 = 0 \tag{1.3}$$

Then,

$$P_x\left[\alpha_0\left(T - T_0\right) + \alpha_{11}P_x^2 + \alpha_{111}P_x^4\right] = 0 \tag{1.4}$$

Because $P_x = 0$ corresponds to a free energy maxima in the ferroelectric phase, the spontaneous polarization, $P_s$, is obtained from the solution of the equation

$$\alpha_0\left(T - T_0\right) + \alpha_{11}P_s^2 + \alpha_{111}P_s^4 = 0 \tag{1.5}$$

which is

$$P_s^2 = \frac{-\alpha_{11} \pm \sqrt{\alpha_{11}^2 - 4\alpha_0\alpha_{111}(T - T_0)}}{2\alpha_{111}} \tag{1.6}$$

Obviously, for either the first- or the second-order phase transitions, the negative square root should be eliminated, thus leading to

$$P_s = \sqrt{\frac{-\alpha_{11} + \sqrt{\alpha_{11}^2 - 4\alpha_0\alpha_{111}(T - T_0)}}{2\alpha_{111}}} \tag{1.7}$$

If $\alpha_{11} = 0$, the spontaneous polarization is similarly given by

$$P_s = \sqrt{-\frac{\alpha_0(T - T_0)}{\alpha_{111}}} \tag{1.8}$$

The hysteresis loop, i.e. $P_x$ versus $E_x$, can be readily derived from the free energy expansion by adding an electrostatic term, $E_x P_x$, as follows:

$$\Delta G = \frac{1}{2}\alpha_0 \left(T - T_0\right) P_x^2 + \frac{1}{4}\alpha_{11} P_x^4 + \frac{1}{6}\alpha_{111} P_x^6 - E_x P_x \tag{1.9}$$

Therefore,

$$\frac{\partial(\Delta G)}{\partial P_x} = \alpha_0 \left(T - T_0\right) P_x + \alpha_{11} P_x^3 + \alpha_{111} P_x^5 - E_x = 0 \tag{1.10}$$

Accordingly,

$$E_x = \alpha_0 \left(T - T_0\right) P_x + \alpha_{11} P_x^3 + \alpha_{111} P_x^5 = 0 \tag{1.11}$$

Plotting $E_x$ as a function of $P_x$ and reflecting the graph about the 45° line will result in a curve with "S" shape. The central part of the "S" corresponds to a free energy local maximum, because there is $\partial^2(\Delta E)/\partial P_x^2 < 0$. By eliminating this region and connecting the top and bottom portions of the "S" curve by vertical lines at the discontinuities, the hysteresis loop is obtained.

Since ferroelectric materials have the highest performances in terms of piezoelectric and pyroelectric properties, they are promising candidates for related applications of mechanical and thermal energy harvesting. At the same time, ferroelectric materials also have very interesting electrocaloric effect (ECE), which can be used for refrigeration applications, while their photovoltaic effect has been paid new attention in recent years. Therefore, in the following sections, these four types of applications of ferroelectric materials, closely related to energy conversion and harvesting, will be discussed, with a focus on more theoretical considerations.

## 1.2 Piezoelectric Mechanical Energy Harvesting

### 1.2.1 Piezoelectricity

The word "piezoelectricity" is derived from the Greek "*piezein,*" which means to "squeeze" or "press" [4]. There are two piezoelectric effects: (i) direct effect and (ii) converse effect. Direct effect (also known as generator) is identified as the phenomenon where electrical charge (variation in polarization) is generated due to the application of an external mechanical stress, while the converse effect

(also known as motor) is defined as the mechanical deformation because of the application of an electrical field. In this respect, piezoelectric energy harvesting is the use of the direct effect (generator).

Properties of piezoelectric materials are generally characterized by $k_p$, $k_{33}$, $d_{33}$, $d_{31}$, and $g_{33}$. The $k$ factors (e.g. $k_{33}$, $k_{31}$, and $k_p$), which are also called piezoelectric coupling factors, are convenient and direct measurements of the overall strength of the electromechanical effects, i.e. the ability of the ceramic transducer to convert one form of energy to another. They are defined as the square root of the ratio of energy output in electrical form to the total mechanical energy input (direct effect), or the square root of the ratio of the energy available in mechanical form to the total electrical energy input (converse effect). Because the conversion of electrical to mechanical energy (or vice versa) is always incomplete, $k$ is always less than unity. Commonly used as a figure-of-merit for piezoelectrics, the higher $k$ values are most desirable and constantly sought after in new materials. For ceramics, $k_p$ is a typical measure used to compare piezoelectric properties of ferroelectric materials – values ranging from 0.35 for $BaTiO_3$ to as high as 0.72 for PLZT [4].

The $d$ coefficients are called piezoelectric coefficients, having magnitudes of $\times 10^{12}\,C\,N^{-1}$ (or $pC\,N^{-1}$) for the direct effect and $\times 10^{-12}\,m\,V^{-1}$ (or $pm\,V^{-1}$) for the converse effect, respectively. The subscript is used to describe the relative direction of inputs and outputs. For example, $d_{31}$ means that this piezoelectric coefficient relates to the generation of polarization (direct effect) in the electrodes perpendicular to the vertical direction (3) and to the stress mechanically applied in the lateral direction (1), while $d_{33}$ indicates the polarization generated in the vertical direction (3) when the stress is applied in the same direction. There are also other similar symbols [4].

The $g$ factors are called open-circuit coefficients, another parameter used to evaluate piezoelectric ceramics for their ability to generate a large voltage per unit of input stress. The $g$ constant is related to the $d$ constant: $g = d/K\varepsilon_0$ ($K$ is the relative dielectric constant and $\varepsilon_0$ is the dielectric constant of free space that equals unity). High-$g$-constant piezoelectric ceramics are usually ferroelectrically hard materials whose polarizations are not readily switched and thus they possess lower $K$ values.

Ferroelectric materials can be grouped into four subcategories according to their crystal structures: perovskite group, pyrochlore group, tungsten-bronze group, and bismuth layer structure group, among which the perovskite group is the most important and thus the most widely studied. Perovskite is usually expressed as $ABO_3$. A typical $ABO_3$ unit cell structure is shown in Figure 1.2, taking $PbTiO_3$ as an example [4]. It consists of a corner-linked network of oxygen octahedron, creating an octahedral cage (B-site) and the interstices (A-sites). $Ti^{4+}$ ions occupy the B-site while $Pb^{2+}$ ions occupy the A-site. Figure 1.2 also shows the paraelectric and ferroelectric states of $PbTiO_3$. Most ferroelectric materials undergo a structural phase transition from a high temperature paraelectric phase into a low-temperature ferroelectric phase. The paraelectric phase always has a higher symmetry than the ferroelectric phase. The temperature of the phase transition is called the Curie temperature ($T_C$). Different ferroelectric materials have different values of $T_C$, which can be either lower than liquid nitrogen (LN)

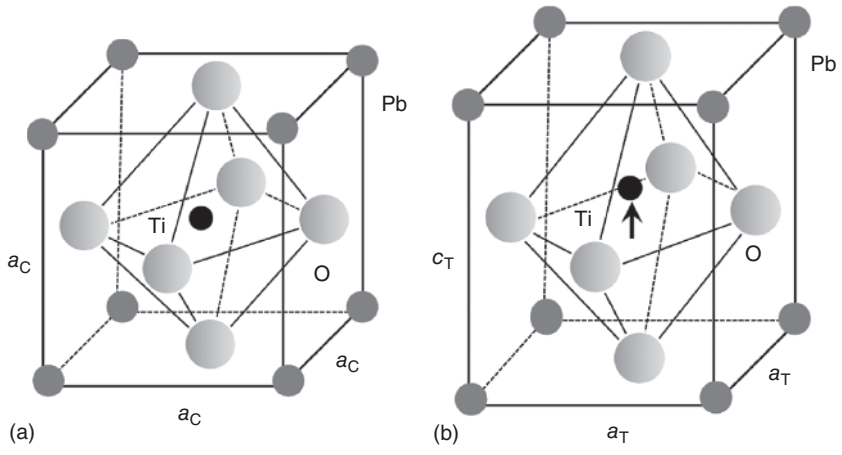


**Figure 1.2** Schematic perovskite structure of $PbTiO_3$, with cubic (C) structure in the paraelectric state ($P_s = 0$) and tetragonal (T) structure in the ferroelectric state ($P_s \neq 0$).

temperature or higher than 1000 °C. For a given material (composition), the $T_C$ is closely related to the microstructure (grain size and distribution, density, porosity and pore size and distribution, impurity, and so on). Generally, the $T_C$ of a given material decreases with decreasing grain size [7].

In the ferroelectric state, the ability of displacement of the central $Ti^{4+}$ ion causes reversibility of polarization. The switch of many adjacent unit cells is referred to as domain reorientation or switching. The homogeneous areas of the material with the same polarization orientation are referred to as domains, with domain walls existing between areas of unlike polarization orientation [5]. For as-prepared piezoelectric ceramics, the domains are randomly oriented and thus the net polarization of materials is zero because of their cancellation effect. Therefore, the as-prepared piezoelectric ceramics have no piezoelectric effect. To show piezoelectric properties, the newly obtained polycrystalline piezoelectric ceramics must be poled at strong external DC electric fields (10–100 kV $cm^{-1}$). Poling is to electrically align the orientation of the randomly distributed domains within the grains and to make ferroelectric ceramics act like a single crystal possessing both ferroelectric and piezoelectric properties. Poling is usually conducted at elevated temperatures, because polarization would be more compliant at high temperatures [5]. After poling during cooling, the applied voltages should be retained until the temperature is sufficiently low.

### 1.2.2 Brief History of Modern Piezoelectric Ceramics

The history of modern piezoelectricity and piezoelectric ceramics is closely related to the history of ferroelectricity and ferroelectric ceramics. The history of ferroelectrics can be tracked back to Rochelle salt (sodium potassium tartrate tetrahydrate, $KNa(C_4H_4O_6)\cdot 4H_2O$), which was synthesized more than 400 years ago, initially for medicinal purpose. It is from this same crystalline material that pyroelectric (thermal-polar), piezoelectric (stress-polar), and ferroelectric

properties were discovered subsequently. Before this discovery, ferroelectricity was only a hypothetical property of solid materials at the turn of the twentieth century. However, the practical application of this material is largely limited due to its water solubility. It was after the discovery of ferroelectric ceramics (barium titanate, $BaTiO_3$) that this class of materials became extremely useful for a variety of applications.

The first ferroelectric ceramic material is $BaTiO_3$ (or BT), which was discovered in the mid-1940s. Before the discovery of $BaTiO_3$, the most widely used materials for capacitors were steatite, mica, $TiO_2$, $MgTiO_3$, and $CaTiO_3$, with the dielectric constant not higher than 100. During the World War II, there was a pressing need for high-dielectric-constant materials to fabricate high-capacitance capacitors. Before any publications were available in the literature, $BaTiO_3$ had already been studied as a high-dielectric-constant material concurrently. In the later open publications, it was concluded that the high dielectric constant in $BaTiO_3$ is due to its ferroelectric properties [4].

The history of ferroelectric ceramics also includes the discovery of lead zirconate titanate ($PbZr_{1-x}Ti_xO_3$, or PZT) piezoelectric ceramics, the development of transparent electro-optical lead lanthanum zirconate titanate ($Pb_{1-x}La_xZr_{1-y}Ti_yO_3$, or PLZT), the research on lead magnesium niobate ($PbMg_{1/3}Nb_{2/3}O_3$, or PMN) relaxor ferroelectric ceramics, and the discovery of many other non-perovskite ferroelectric ceramics [4]. Among these, PZT has been demonstrated to possess the best performance as piezoelectric ceramics.

Recently, there has been a concern with PZT due to the toxicity of Pb. Regulations and legislations have been established globally to restrict the use of lead-containing materials. For example, according to the directive for the Restriction of the use of certain Hazardous Substances (RoHS) in electrical and electronic equipment adopted by the European Parliament in the year 2006, the maximum allowed concentration of lead is established to be 0.1 wt% in homogeneous materials for electrical and electronic equipment used in households as well as industry. Therefore, lead-containing piezoelectric materials will be prohibited eventually. Similar regulations have been established worldwide. As a consequence, there is significantly increasing interest in developing lead-free piezoelectric ceramics all around the world. Although major progress has been made in materials research [8], there are still obstacles blocking the successful industrial implementation of lead-free piezoelectric ceramics. Key problems are their poor piezoelectric properties and fatigue degradation. Therefore, PZT will still be a dominant material for piezoelectric applications in most areas.

### 1.2.3 Principle of Piezoelectric Effect for Mechanical Energy Harvesting

The harvesting of mechanical energy is to convert it into electrical energy, which requires a mechanical system that couples motion or vibration to a transduction mechanism. The mechanical system should be designed to be able to maximize the coupling between the mechanical energy sources and the transduction mechanism, depending on the characteristics of the environmental motions. For example, energy due to vibration can be converted by using inertial generators,

with the mechanical component attached to an inertial frame that acts as a fixed reference. The inertial frame transmits the vibrations to a suspended inertial mass to produce a relative displacement between them. Systems such as this usually have a resonant frequency, which can be designed to match the characteristic frequency of the environmental motions. Detailed analysis on mechanisms of mechanical energy harvesting can be found in the open literature [9, 10]. A brief description is presented here.

These inertia-based generators can be well described as second-order spring-mass systems. For a system with a seismic mass of $m$ on a spring with a stiffness of $k$, its energy loss, consisting of parasitic loss, $c_p$, and electric energy generated by the transduction mechanism, $c_e$, can be represented by the damping coefficient, $c_T$. The system is excited by an external sinusoidal vibration, $y(t) = Y\sin(\omega t)$. At resonant frequency, there is a net displacement, $z(t)$, between the mass and the frame. If the mass of the vibration source is greatly larger than that of the seismic mass, the latter can be ignored. If the external excitation is harmonic, the differential equation of the motion is given by

$$m\ddot{z}(t) + c\dot{z}(t) + kz(t) = -m\ddot{y}(t) \tag{1.12}$$

Standard solution for the mass displacement will be

$$z(t) = \frac{\omega^2}{\sqrt{\left(\frac{k}{m} - \omega^2\right)^2 + \left(\frac{c_T\omega}{m}\right)^2}} y\sin(\omega t - \varphi) \tag{1.13}$$

where $\phi$ is the phase angle, given by

$$\varphi = \tan^{-1}\left(\frac{c_T\omega}{k - \omega^2 m}\right) \tag{1.14}$$

Energy conversion can be maximized when the excitation frequency matches the natural frequency of the system, $\omega_n$, given by

$$\omega_n = \sqrt{\frac{k}{m}} \tag{1.15}$$

The power dissipated with the system is

$$P_d = \frac{m\zeta_T Y^2\left(\frac{\omega}{\omega_n}\right)^3\omega^3}{\left[1 - \left(\frac{\omega}{\omega_n}\right)^2\right]^2 + \left[2\zeta_T\left(\frac{\omega}{\omega_n}\right)\right]^2} \tag{1.16}$$

where $\zeta_T$ is the total damping ratio, which is $\zeta_T = c_T/2m\omega_n$. Maximum power is achieved when the system is operated at $\omega_n$, while $P_d$ can be expressed as

$$P_d = \frac{mY^2\omega_n^3}{4\zeta_T} \tag{1.17}$$

$$P_d = \frac{mA^2}{4\omega_n\zeta_T} \tag{1.18}$$

where $A$ is the excitation acceleration level, with $A = \omega_n^2 Y$. Noting that these are steady-state solutions, power will not tend to infinity when the damping ratio

approaches zero. The maximum power generation can be evaluated by considering the parasitic and system damping ratio, which is given by

$$P_{\mathrm{e}} = \frac{m\zeta_{\mathrm{e}}A^2}{4\omega_{\mathrm{n}}(\zeta_{\mathrm{p}} + \zeta_{\mathrm{e}})^2} \tag{1.19}$$

$P_{\mathrm{e}}$ is maximized at $\zeta_{\mathrm{p}} = \zeta_{\mathrm{e}}$. When there is sufficient acceleration, increased damping effects will lead to a response with broadened bandwidth, so that the generator will be less sensitive to frequency. An excessive device amplitude can lead to nonlinear behavior of the generator, which will make it difficult to keep the generator working at resonance frequency. For specific applications, both the frequency of the generator and the level of damping should be specifically designed to maximize the power output. The power generation can also be maximized by maximizing the mass of the mechanical structure.

The piezoelectric damping coefficient can be estimated by using the following equation:

$$c_{\mathrm{e}} = \frac{2m\omega_{\mathrm{n}}^2k^2}{2\sqrt{\omega_{\mathrm{n}}^2 + \left(\frac{1}{R_{\mathrm{load}}C_{\mathrm{load}}}\right)^2}} \tag{1.20}$$

where $k$ is the piezoelectric coupling factor of the materials, while $R_{\mathrm{load}}$ and $C_{\mathrm{load}}$ are load resistance and capacitance. At maximum power generation, there is optimal load, given by

$$R_{\mathrm{opt}} = \frac{1}{\omega_{\mathrm{n}}C}\frac{2m\omega_{\mathrm{n}}^2k^2}{\sqrt{4\zeta_{\mathrm{p}}^2 + k^4}} \tag{1.21}$$

Specifically, for piezoelectric materials, the mechanical and electrical behaviors can be described by using the following linear constitutive equations:

$$S_{ij} = s_{ijkl}^{\mathrm{E}}T_{kl} + d_{kij}E_k \tag{1.22}$$

$$D_i = d_{ikl}^{\mathrm{E}}T_{kl} + \varepsilon_{ik}^{\mathrm{T}}E_k \tag{1.23}$$

Each of the subscripts $i$, $j$, $k$, and $l$ can take values of 1, 2, and 3. $S$ and $T$ are strain and stress tensors, respectively. The stresses, represented by $T$ with a unit of $\mathrm{N\,m^{-2}}$, are induced by the mechanical and electrical effects. $D$ and $E$ are the electric displacement and electric field vectors, with units of $\mathrm{C\,m^{-2}}$ and $\mathrm{V\,m^{-1}}$, respectively. Also, $s^{\mathrm{E}}$ is the elastic compliance matrix evaluated at a constant electric field with a unit of $\mathrm{m^2\ N^{-1}}$, $d$ is a matrix of piezoelectric strain coefficients with a unit of $\mathrm{m\,V^{-1}}$, and $\varepsilon^{\mathrm{T}}$ is a matrix of permittivity values that are evaluated at a constant stress with a unit of $\mathrm{N\,V^{-2}}$. In Eqs. (1.22) and (1.23), $d$ represents the charge created by an external force in the absence of an electric field (short circuit electrical condition) or the displacement caused by an applied voltage in the absence of an applied force (stress-free mechanical condition).

For piezoelectric composite materials, effective electromechanical coupling factor is used, which is given by

$$k_{\mathrm{eff}} = \sqrt{1 - \left(\frac{F_{\mathrm{r}}}{F_{\mathrm{a}}}\right)^2} \tag{1.24}$$

where $F_r$ is the resonance frequency (Hz) and $F_a$ is the antiresonance frequency (Hz) of a piezoelectric cantilever beam. The voltage coefficient, $g$ (V m N$^{-1}$), is given by

$$g = \frac{d}{\varepsilon_T} \tag{1.25}$$

The mechanical quality factor, $Q_M$, is defined as [11]

$$Q_M = 2\pi \frac{\text{energy stored/cycle}}{\text{energy dissipated/cycle}} \tag{1.26}$$

The amount of energy stored in a piezoelectric device, $E_C$, is given by

$$E_C = \frac{1}{2} CV^2 \tag{1.27}$$

where $C$ is capacitance of the piezoelectric element and $V$ is the voltage produced.

The maximum efficiency of the piezoelectric devices can also be estimated by the following equation:

$$\eta = \frac{\frac{1}{2}\left(\frac{k^2}{1-k^2}\right)}{\frac{1}{Q_M} + \frac{1}{2}\left(\frac{k^2}{1-k^2}\right)} \tag{1.28}$$

This equation indicates that the efficiency can be increased by increasing $k$ and $Q_M$, which are properties of the piezoelectric materials. Therefore, selection of materials is a very important step toward energy harvesters with high efficiencies. This is also the reason why PZT has been the most promising piezoelectric material for mechanical energy harvesting applications.

## 1.3 Pyroelectric Thermal Energy Harvesting

### 1.3.1 Principle of Pyroelectric Effect

As stated earlier, pyroelectric effect is defined as the phenomenon of change in polarization of a material induced by change in temperature [12, 13]. For a single domain ferroelectric material, there are localized charges that are present on the two end surfaces, due to the alignment of the polarization. At thermal equilibrium state, these localized charges are shielded by the free charges with same quantity but opposite signs, so that there is no net electricity produced in the ferroelectric material. However, when there is a change in temperature, the polarization of the material is changed. As a result, the free charges cannot completely shield the localized charges and thus there will be free charges at the surfaces, which leads to the formation of an electric field nearby. The presence of the electric field is indicated by the fact that the material can attract or repel charged particles. If the surfaces are connected with external circuit, there will be electric current flowing through it. The directions of the electrical currents corresponding to heating and cooling are opposite.

Similar to the piezoelectric of ferroelectric materials, the charge of current of pyroelectric effects is closely related to the change in polarization, which thus

breaks the equilibrium with free charges, so that the amount of surface charges is increased and decreased corresponding to heating and cooling, respectively. The difference is that the change in polarization of pyroelectric effect is caused by the change in temperature, while that of piezoelectric effect is caused by mechanical stress. The physics of pyroelectric effect has been well described in the open literature [12–15]. A brief description of various physical quantities related to pyroelectric effect and pyroelectric materials is presented in this subsection.

The pyroelectric effect of a pyroelectric material is characterized by the pyroelectric coefficient, a parameter that measures the pyroelectric efficiency of the material. With a small change in temperature, $\Delta T$, the variation induced can be given by

$$\Delta P = p\Delta T \tag{1.29}$$

where $p$ is the pyroelectric coefficient, which is a vector and has three nonzero components, with unit of $\mathrm{C\,m^{-2}\,K^{-1}}$:

$$p_m = \frac{\partial P_m}{\partial T}, \quad m = 1, 2, 3 \tag{1.30}$$

The sign of the pyroelectric coefficient is determined with respect to the piezoelectric axis of the piezoelectric crystal. According to IRE standards, the end of a crystal axis with positive charge under tension is defined as the positive end. When a pyroelectric crystal is heated, if there is positive charge produced at the positive side, the pyroelectric coefficient is defined to be positive; otherwise, it is negative. Generally, because the spontaneous polarization of ferroelectric materials decreases with increasing temperature, the pyroelectric coefficient is usually negative. However, there are also exceptions; for example, the spontaneous polarization of Rochelle salt increases with increasing the temperature slightly below its Curie point.

Because the best pyroelectric materials are piezoelectric materials, the deformation of a pyroelectric material due to change in temperature can induce variation in polarization, which also contributes to pyroelectric effect. Therefore, it is important to pay attention to mechanical boundary conditions and the ways of change variation.

Under uniform heating or cooling, depending on mechanical boundary conditions, there are two types of pyroelectric effects. Under constant strain (sample is clapped), only the variation in polarization induced by temperature change contributes to pyroelectric effect. It is called primary pyroelectric effect or constant strain pyroelectric effect. Usually, it is difficult to maintain a constant strain. In other words, samples are in free-strain state or constant stress state. In this case, the variation in polarization induced by the mechanical deformation of the sample due to thermal expansion will be added on top of the primary pyroelectric effect. This additional pyroelectric effect at uniform temperature is called secondary pyroelectric effect. Therefore, the pyroelectric coefficient of a material under constant stress is the summation of the primary and secondary coefficients, and is known as the total pyroelectric coefficient. However, in practice, the pyroelectric element in a pyroelectric device is neither under constant strain nor under constant stress [16]. For example, it is only strained in

one specific direction and free in other directions. In this case, the pyroelectric coefficient is called a partially strained coefficient.

If a pyroelectric sample is heated or cooled in a nonuniform manner, it will experience a stress gradient, which also contributes to the pyroelectric effect, through piezoelectric effect. This nonuniform heating- or cooling-induced pyroelectric effect is called a tertiary effect or false effect. It is named false effect because piezoelectric materials, including those outside the 10 polar point group, have such an effect under nonuniform heating or cooling. Those piezoelectric materials actually have no pyroelectric effect. As a result, the heating or cooling should be uniform to exclude the false pyroelectric effect.

### 1.3.2 Pyroelectric Coefficient and Electrocaloric Coefficient

The thermodynamic states of elastic dielectrics can be described with temperature $T$, entropy $S$, electric field $\boldsymbol{E}$, electric displacement $D$, strain $X$, and stress $x$. With $T$, $E$, and $X$ as independent variables, the differential form of electric displacement can be expressed as

$$\begin{aligned} \mathrm{d}D_m &= \left(\frac{\partial D_m}{\partial X_i}\right)_{E,T} \mathrm{d}X_i + \left(\frac{\partial D_m}{\partial E_n}\right)_{X,T} \mathrm{d}E_n + \left(\frac{\partial D_m}{\partial T}\right)_{E,X} \mathrm{d}T \\ &= \mathrm{d}_{mi}^{E,T}\, \mathrm{d}X_i + \varepsilon_{mn}^{X,T}\, \mathrm{d}E_n + p_m^{E,X}\, \mathrm{d}T \end{aligned} \tag{1.31}$$

where the subscript $m = 1 - 3$ and $i = 1 - 6$, while the superscript means that the physical quantities are kept constant. On the right-hand side, the first and the second terms are piezoelectric and dielectric characteristics, whereas the third term is the pyroelectric property of a material.

When $\mathrm{d}X_i = 0$ and $\mathrm{d}E_n = 0$,

$$\mathrm{d}D_m = p_m^{E,X}\, \mathrm{d}T \tag{1.32}$$

With independent variables, $T$, $E$, and $X$, the characteristic functions of Gibbs free energy become

$$G = U - TS - X_i x_i - E_m D_m \tag{1.33}$$

According to thermodynamic first and second laws,

$$\mathrm{d}G = -x_i\, \mathrm{d}X_i - D_m\, \mathrm{d}E_m - S\, \mathrm{d}T \tag{1.34}$$

The differential form of the Gibbs free energy, with respect to $T$, $E$, and $X$, can be expressed as

$$\mathrm{d}G = \left(\frac{\partial G}{\partial X_i}\right)_{E,T} \mathrm{d}X_i + \left(\frac{\partial G}{\partial E_m}\right)_{X,T} \mathrm{d}E_m + \left(\frac{\partial G}{\partial T}\right)_{E,X} \mathrm{d}T \tag{1.35}$$

By comparing Eqs. (1.34) and (1.35), we have

$$\left(\frac{\partial G}{\partial E_m}\right)_{X,T} = -D_m \tag{1.36}$$

$$\left(\frac{\partial G}{\partial T}\right)_{E,X} = -S \tag{1.37}$$

$$\left(\frac{\partial^2 G}{\partial E_m \, \partial T}\right)_X = -\left(\frac{\partial D_m}{\partial T}\right)_{E,X} = -p_m^{E,X} \tag{1.38}$$

$$\left(\frac{\partial^2 G}{\partial E_m \, \partial T}\right)_X = -\left(\frac{\partial S}{\partial E_m}\right)_{X,T} \tag{1.39}$$

The pyroelectric coefficient is thus defined in Eq. (1.38), whereas Eq. (1.39) describes the change in entropy induced by an external electric field, which is known as EC coefficient. Therefore, ECE is inverse pyroelectric effect, and thus

$$p_m^{E,X} = -\left(\frac{\partial S}{\partial E_m}\right)_{X,T} \tag{1.40}$$

It means that the pyroelectric coefficient under constant electric field and stress is equal to the ECE under constant stress and temperature.

With independent variables, $T$, $E$, and $x$, the differential form of electric displacement can be expressed as

$$\begin{aligned} \mathrm{d}D_m &= \left(\frac{\partial D_m}{\partial x_i}\right)_{E,T} \mathrm{d}x_i + \left(\frac{\partial D_m}{\partial E_n}\right)_{x,T} \mathrm{d}E_n + \left(\frac{\partial D_m}{\partial T}\right)_{E,x} \mathrm{d}T \\ &= e_{mi}^{E,T} \, \mathrm{d}x_i + \varepsilon_{mn}^{x,T} \, \mathrm{d}E_n + p_m^{E,x} \, \mathrm{d}T \end{aligned} \tag{1.41}$$

Under constant strain and electric field,

$$\mathrm{d}D_m = p_m^{E,x} \, \mathrm{d}T \tag{1.42}$$

Similarly, with independent variables, $T$, $E$, and $x$, the characteristic functions of Gibbs free energy are written as

$$\mathrm{d}G_2 = X_i \, \mathrm{d}x_i - D_m \, \mathrm{d}E_m - S \, \mathrm{d}T \tag{1.43}$$

Similar to Eq. (5.7),

$$\mathrm{d}G_2 = \left(\frac{\partial G_2}{\partial x_i}\right)_{E,T} \mathrm{d}x_i + \left(\frac{\partial G_2}{\partial E_m}\right)_{x,T} \mathrm{d}E_m + \left(\frac{\partial G_2}{\partial T}\right)_{E,x} \mathrm{d}T \tag{1.44}$$

As a result,

$$\left(\frac{\partial G_2}{\partial E_m}\right)_{x,T} = -D_m \tag{1.45}$$

$$\left(\frac{\partial G_2}{\partial T}\right)_{E,x} = -S \tag{1.46}$$

According to partial derivatives,

$$p_m^{E,x} = -\left(\frac{\partial S}{\partial E_m}\right)_{x,T} \tag{1.47}$$

Therefore, the pyroelectric coefficient under constant electric field and strain is equal to the ECE under constant strain and temperature.

The change in entropy of a ferroelectric material is due to the change in ordering of polarization. The higher the degree of ordering, the lower the value of entropy of the system will be. As a consequence, depolarization of a

ferroelectric material leads to an increase in the value of entropy because the degree of ordering of polarization is decreased. Under adiabatic conditions, depolarization results in a decrease in temperature, which is the reason why ECE can be used for refrigeration through depolarization.

### 1.3.3 Primary and Secondary Pyroelectric Coefficient

At zero electric field (constant electric field), electric displacement is only a function of strain and temperature, while strain is only a function of stress and temperature, i.e.

$$\mathrm{d}D_m = \left(\frac{\partial D_m}{\partial x_i}\right)_T \mathrm{d}x_i + \left(\frac{\partial D_m}{\partial T}\right)_x \mathrm{d}T \tag{1.48}$$

$$\mathrm{d}x_i = \left(\frac{\partial x_i}{\partial X_j}\right)_T \mathrm{d}X_j + \left(\frac{\partial x_i}{\partial T}\right)_X \mathrm{d}T \tag{1.49}$$

With $\mathrm{d}X_j = 0$, combining Eqs. (5.20) and (5.21) leads to

$$\mathrm{d}D_m = \left[\left(\frac{\partial D_m}{\partial x_i}\right)_T \left(\frac{\partial x_i}{\partial T}\right)_X + \left(\frac{\partial D_m}{\partial T}\right)_x\right] \mathrm{d}T \tag{1.50}$$

Rearranging Eq. (5.22),

$$\left(\frac{\partial D_m}{\partial T}\right)_X = \left(\frac{\partial D_m}{\partial T}\right)_x + \left(\frac{\partial D_m}{\partial x_i}\right)_T \left(\frac{\partial x_i}{\partial T}\right)_X \tag{1.51}$$

where the left-hand side term is the total pyroelectric coefficient, while the first term on the right-hand side is the primary pyroelectric coefficient and the second term is the secondary coefficient.

In Eq. (1.51),

$$\left(\frac{\partial D_m}{\partial x_i}\right)_T = e_{mi} \tag{1.52}$$

$$\left(\frac{\partial x_i}{\partial T}\right)_X = \alpha_i \tag{1.53}$$

where $e_{mi}$ and $\alpha_i$ are the piezoelectric constant and thermal expansion coefficient, respectively. Therefore, Eq. (1.51) becomes

$$p_m^X = p_m^x + e_{mi}^T \alpha_i^X \tag{1.54}$$

where the second term on the right-hand side means that the secondary pyroelectric coefficient is the product of the piezoelectric constant and the thermal expansion coefficient.

If Eq. (1.51) is rewritten as

$$\left(\frac{\partial D_m}{\partial T}\right)_X = \left(\frac{\partial D_m}{\partial T}\right)_x + \left(\frac{\partial D_m}{\partial X_i}\right)_T \left(\frac{\partial X_i}{\partial x_j}\right)_T \left(\frac{\partial x_j}{\partial T}\right)_X \tag{1.55}$$

the following expression for total pyroelectric coefficient results:

$$p_m^X = p_m^x + d_{mi}^T c_{ij}^T \alpha_j^X \tag{1.56}$$

where the second term on the right-hand side means that the secondary pyroelectric coefficient is the product of piezoelectric constant, elastic stiffness, and thermal expansion coefficient. In most cases, the primary coefficient is the main contributor of pyroelectric materials.

### 1.3.4 Tertiary Pyroelectric Coefficient and Other Aspects

As stated before, under the condition of nonuniform heating or cooling without mechanical stress, the total pyroelectric coefficient consists of primary, secondary, and tertiary coefficients. The tertiary pyroelectric coefficient is attributed to thermal stress, whose contribution to the change in polarization is $d_{mnp}X_{np}(r, t)$, where $d_{mnp}$ and $X_{np}$ are the piezoelectric constant and thermal stress component, while $r$ and $t$ are displacement and time, respectively [17]. Owing to the difficulty in characterization of thermal stress, which is a function of location and time, it is a challenge to accurately measure the tertiary pyroelectric coefficient.

When elastic Gibbs free energy $G_1$ is used as a characteristic function, with variables such as stress and electric field being one dimensional,

$$\mathrm{d}G_1 = -S\,\mathrm{d}T + x\,\mathrm{d}X + E\,\mathrm{d}D \tag{1.57}$$

Taking the derivative of Eq. (1.57),

$$\frac{\partial G_1}{\partial D} = E \tag{1.58}$$

$$\frac{\partial^2 G_1}{\partial D^2} = \frac{1}{\varepsilon} \tag{1.59}$$

At temperatures near Curie point,

$$\frac{\partial G_1}{\partial D} = \alpha D + \beta D^3 + \gamma D^5 \tag{1.60}$$

which can be rewritten as

$$E = \alpha_0(T - T_0)D + \phi(D) \tag{1.61}$$

where $\varphi(D)$ represents all higher order terms and $\alpha_0 = 1/(\varepsilon_0 C)$, with $C$ being the Curie constant, which leads to

$$\frac{\partial E}{\partial T} = \alpha_0 D \tag{1.62}$$

Therefore, if $E = 0$ and $D = P_s$, at temperatures near the Curie point,

$$\alpha_0(T - T_0)P_s + \phi(P_s) = 0 \tag{1.63}$$

i.e.

$$\left.\frac{\partial G_1}{\partial D}\right|_{D=P_s} = \alpha_0(T - T_0)P_s + \phi(P_s) = 0 \tag{1.64}$$

$$\frac{\mathrm{d}}{\mathrm{d}T}\left(\frac{\partial G_1}{\partial D}\right)_{D=P_s} = \left.\frac{\partial^2 G_1}{\partial D^2}\right|_{D=P_s}\frac{\mathrm{d}D}{\mathrm{d}T} + \left.\frac{\partial^2 G_1}{\partial T\,\partial D}\right|_{D=P_s} = 0 \tag{1.65}$$

Comparing Eqs. (1.59) and (1.62),

$$\left.\frac{\partial^2 G_1}{\partial T\,\partial D}\right|_{D=P_s} = \left.\frac{\partial E}{\partial T}\right|_{D=P_s} = \alpha_0 P_s \tag{1.66}$$

Substituting Eq. (1.66) in Eq. (1.65),

$$\frac{p}{\varepsilon_r} + \alpha_0 P_s = 0 \tag{1.67}$$

where $p = \mathrm{d}D/\mathrm{d}T$, which is the pyroelectric coefficient, thus leading to

$$\frac{p}{\varepsilon_r} = \frac{P_s}{C} \tag{1.68}$$

which correlates the pyroelectric coefficient with Curie constant, spontaneous polarization, and permittivity of a pyroelectric material. With this relationship, the pyroelectric coefficient can be estimated by using the Curie constant, and vice versa. It is necessary to mention that the temperature range of validity of the formula should not be too wide.

It has been found that although there is a significant difference in the pyroelectric coefficient and permittivity among various pyroelectric/ferroelectric materials, the value of the ratio $p\varepsilon_r^{-1/2}$ is nearly constant for most ferroelectric materials, with a temperature range across room temperature. This phenomenon has been well explained by using ferroelectric phenomenological theories. With Devonshire's assumption, the elastic Gibbs free energy $G_1$ can be expressed as

$$\frac{\partial G_1}{\partial D} = \alpha_0(T - T_0)D + \beta D^3 + \gamma D^5 = E \tag{1.69}$$

Near the Curie point, with $E = 0$ and $D = P_s$,

$$\alpha_0(T - T_0)P_s + \beta P_s^3 + \gamma P_s^5 = 0 \tag{1.70}$$

The solutions of this equation are

$$P_s^2 = -\frac{\beta}{2\gamma}\left\{1 + \left[1 - 4\alpha_0\gamma\beta^{-2}(T - T_0)\right]^{1/2}\right\} \tag{1.71}$$

$$P_s^2 = -\frac{\beta}{2\gamma}\left\{1 - \left[1 - 4\alpha_0\gamma\beta^{-2}(T - T_0)\right]^{1/2}\right\} \tag{1.72}$$

where Eq. (1.71) is for $\beta < 0$ and Eq. (1.72) is for $\beta > 0$. For second-order phase transition with $\beta > 0$, Eq. (1.71) becomes

$$P_s^2 = -\frac{\beta}{2\gamma} - \frac{\beta}{2\gamma}\left[1 + \frac{4\gamma(T_0 - T)}{\varepsilon_0 C\beta^2}\right]^{1/2} \tag{1.73}$$

For first-order phase transition, it is

$$P_s^2 = -\frac{|\beta|}{2\gamma} - \frac{|\beta|}{2\gamma}\left[1 - \frac{4\gamma(T_0 - T)}{\varepsilon_0 C\beta^2}\right]^{1/2} \tag{1.74}$$

The pyroelectric coefficient can be derived from their derivatives with respect to temperature, given by

$$p = (2P_s\varepsilon_0 C|\delta|)^{-1}\left[1 + \frac{4\gamma(T_0 - T)}{C\beta^2}\right]^{1/2} \tag{1.75}$$

With Eq. (1.68), on multiplying the two sides of Eq. (1.75) by $p/\varepsilon_r$ and $P_s/C$, respectively,

$$\frac{p^2}{\varepsilon_r} = P_0^2(2\varepsilon_0 C T_0)^{-1}\left[1 + \frac{4P_0^2\gamma}{|\beta|}\left(1 - \frac{T}{T_0}\right)\right]^{1/2} \tag{1.76}$$

where

$$P_s^2 = T_0\frac{\partial P_s^2}{\partial T}\bigg|_{T\le T_0} = \frac{2T_0}{\varepsilon_0 C|\beta|} \tag{1.77}$$

When $T \approx T_0$, Eq. (1.76) can be simplified as

$$p\varepsilon_r^{-1/2} \approx P_0(2CT_0)^{-1/2} \tag{1.78}$$

The equation can be used to understand the abovementioned phenomenon, which has been taken as a reference to estimate the performance of pyroelectric materials.

### 1.3.5 Pyroelectric Effect versus Phase Transition

For ferroelectric pyroelectric materials, there are two types of phase transition, where a peak is observed in the pyroelectric coefficient curve with temperature [18]. Ferroelectric–paraelectric transition is the most important phase occurring in ferroelectric pyroelectric materials. During this phase transition, there is a sharp change in spontaneous polarization.

For first-order ferroelectrics, at temperatures slightly higher than Curie point $T_C$, an external electric field may induce the appearance of a ferroelectric phase, where the temperature of the maximized variation in polarization, corresponding to the peak of pyroelectric coefficient, increases with increasing magnitude of external applied electric field [19]. This phenomenon can be readily explained with Eq. (1.69). According to reduced electric displacement $d$, electric field $e$, and temperature $t$,

$$d = -(2\gamma/|\beta|)^{1/2}D \tag{1.79}$$

$$e = -8(2\gamma^3/|\beta|^5)^{1/2}E \tag{1.80}$$

$$t = 4\alpha_0\beta^{-2}(T - T_0) \tag{1.81}$$

Then, Eq. (1.69) can be simplified as

$$e = 2d^5 - 4d^3 + 2td \tag{1.82}$$

According to the definition of pyroelectric coefficient, we have reduced the pyroelectric coefficient, given by

$$\frac{\partial d}{\partial t} = \left(4d - 4d^3 - \frac{e}{2d^2}\right)^{-1} = \frac{d}{6d^2 - 5d^4 - t} \tag{1.83}$$

For second-order phase transition ferroelectrics, there is no electric-field-induced phase transition [18]. The application of an external electric field only suppresses the curve of dielectric constant versus temperature and thus the temperature corresponding to the pyroelectric coefficient peak is kept unchanged. However, the magnitude of pyroelectric coefficient decreases with increasing magnitude of electric field. By omitting the higher order term, Eq. (1.69) is simplified as

$$E = \alpha_0(T - T_0)D + \beta D^3 \tag{1.84}$$

where $T_0 = T_C$. Because the electric field is constant, the derivative of Eq. (1.84) is

$$0 = \left[\alpha_0(T - T_0) + 3\beta D^2\right] \mathrm{d}D + \alpha_0 D \,\mathrm{d}T \tag{1.85}$$

Therefore, the pyroelectric coefficient is given by

$$p = \left(\frac{\partial D}{\partial T}\right)_{E,X} = \frac{-\alpha_0 D_0}{\alpha_0(T - T_0) + 3\beta D^2} \tag{1.86}$$

where $D_0$ is the electric displacement induced by the electric field $E$ at temperature $T$, which can be calculated by using Eq. (1.84). There are three special cases, where we have

$$D_0 \approx E\left[\alpha_0(T - T_0)\right]^{-1}, \quad T \gg T_0 \tag{1.87}$$

$$D_0 \approx \left[\alpha_0\beta^{-1}(T_0 - T)\right]^{-1/2}, \quad T \ll T_0 \tag{1.88}$$

$$D_0 \approx (\alpha_0/\beta)^{1/3}, \quad T = T_0 \tag{1.89}$$

Substituting Eqs. (1.87)–(1.89) in Eq. (1.86), with $p_0$ being the pyroelectric coefficient at $T = T_0$, we have

$$p = E\alpha_0^{-1}(T - T_0)^{-2}, \quad T \gg T_0 \tag{1.90}$$

$$p = \frac{1}{2}\alpha_0^{1/2}\beta^{-1/2}(T_0 - T)^{-1/2}, \quad T \ll T_0 \tag{1.91}$$

$$p_0 = \frac{1}{3}\alpha_0/\beta^{-2/3}E^{-1/3}, \quad T = T_0 \tag{1.92}$$

Therefore, below Curie point, the pyroelectric coefficient increases with temperature with $(T_0 - T)^{-1/2}$, while above Curie point, the pyroelectric coefficient decreases with $(T - T_0)^{-2}$. At Curie point, the pyroelectric coefficient is maximized, which is affected by the electric field in terms of magnitude, but without shift in temperature.

Another phase transition is ferroelectric–ferroelectric phase transition, where both magnitude and direction of the spontaneous polarization do not change

in most cases. There are seldom cases where the direction of the polarization does change. In this case, other phase transition related parameters will experience only negligible variation, but pyroelectric effect still has a peak value. Therefore, pyroelectric coefficient has been a sensitive indicator of ferroelectric–ferroelectric phase transition of ferroelectric materials.

When a pyroelectric material is heated or cooled from one temperature to another, it takes time for the polarization to reach a new equilibrium state. Therefore, the response of pyroelectric charges to the variation in temperature is not instantaneous, but with a certain degree of delay, depending on a number of factors, including thermal conductivity and heat capacity of the material, as well as sample dimension and shape. Generally, thermal relaxation time can be expressed as

$$\tau_T = \frac{L^2 c'}{\sigma_T} \tag{1.93}$$

where $c'$ is the heat capacitance per unit volume in $J\,K^{-1}\,m^{-3}$, $L$ is the length in the direction of heat conduction in meters (m), and $\sigma_T$ is thermal conductivity in $J\,K^{-1}\,m^{-1}\,s^{-1}$. Therefore, it is important to have an estimate on $\tau_T$ before discussing the pyroelectric response. It has been acknowledged that, during both the ferroelectric–ferroelectric and ferroelectric–paraelectric phase transitions, ferroelectric materials usually experience a peak in the value of their specific heat, which will also lead to a significant increase in $\tau_T$ [20].

## 1.4 Electrocaloric (EC) Effect of Ferroelectric Materials

When an electric field is applied to a dielectric material it will induce a change in the polarization and consequently a change in the entropy and temperature in the material. Such an electric-field-induced temperature and entropy change in a dielectric material is known as the ECE [1–3].

The ECE is attractive because it may provide a very efficient means to realize solid-state cooling devices for a broad range of applications such as on-chip cooling and temperature regulation for sensors, electronic devices, and medical specimens. Furthermore, refrigeration based on the ECE approach is more environmentally friendly and hence may also provide an alternative to the existing vapor-compression approach.

More recently, ECE of ferroelectric materials has received intensive attention, due to its potential application in the area of energy saving and conversion, with progress that has been well overviewed in the literature [21–24]. It is well known that as a dielectric material is subjected to an external applied field, polarization is induced in the material, thus leading to a variation in entropy and temperature, which is called the ECE [25]. Owing to its potential of achieving solid-state cooling, the ECE has become a worldwide hot research topic. Solid-state cooling could find a wide range of applications, including on-chip cooling and temperature management of electronic devices. Moreover, it can be used to realize refrigeration, with more environment friendliness, so as to replace the currently used vapor-compression technique in the future.

The study of ECE can be traced back to the 1930s when the ECE was first measured experimentally [26]. However, the ECE was too weak to be used for practical applications. It was after the discovery of ferroelectricity in the 1920s that ECE-derived applications started to draw more attention, due to the large polarization required by real device design [27–29]. Besides large polarization, ferroelectric materials for ECE applications should be workable near room temperature, which requires them to have a suitable ferroelectric (F)–paraelectric (P) transition point (Curie temperature or $T_C$), because ECE is maximized just above $T_C$. For example, a $PbZr_{0.95}Ti_{0.05}O_3$ thin film, at temperatures above its F–P phase transition of about 222 °C, exhibited an adiabatic temperature change of as high as 12 °C [30]. Such a large ECE, with an adiabatic temperature change of 12 °C, was also observed in the ferroelectric polymer, poly(vinylidene fluoride–trifluoroethylene) [P(VDF–TrFE)] copolymer [31].

Theoretically, ECE can be related to the pyroelectric effect of ferroelectric materials, through the Maxwell relation, in terms of electric field ($E$) induced adiabatic temperature change, given by [32]

$$\left(\frac{\partial T}{\partial E}\right)_S = \frac{Tp_E}{c_E} \tag{1.94}$$

where $T$ is the temperature, $c_E$ is the volumetric specific heat at a constant electrical field, $S$ is entropy, and $p_E$ is the pyroelectric coefficient at a constant field, $(\partial D/\partial T)_E$, with $D$ being the electric displacement. According to Eq. (1.94), the isothermal entropy change $\Delta S$ and adiabatic temperature change $\Delta T$, as the external applied field is changed from $E_1$ to $E_2$, can be expressed as

$$\Delta S = -\int_{E_1}^{E_2} \left(\frac{\partial D}{\partial T}\right)_{S,E} \mathrm{d}E \tag{1.95}$$

$$\Delta T = -\int_{E_1}^{E_2} \frac{T}{c_E}\left(\frac{\partial D}{\partial T}\right)_{S,E} \mathrm{d}E \tag{1.96}$$

where $D = \varepsilon_0 E + P$, with $P$ being the polarization and $\varepsilon_0$ the vacuum dielectric constant. To achieve large values of $\Delta S$ and $\Delta T$, a sufficiently high pyroelectric coefficient should be available over a wide range of both electric field and temperature. Usually, ferroelectric materials exhibit high pyroelectric effect at temperatures that are near the F–P transition point. Also, it is possible to obtain a large $\Delta T$, even though $\Delta S$ is not very high, as long as the material has a sufficiently low value of $c_E$. However, practical refrigeration applications require a relatively high $\Delta S$. Currently, ECE has been mostly studied according to the Maxwell relationships, as described in Eqs. (1.95) and (1.96), i.e. electric displacement $D$ as a function of temperature $T$ at different electric fields.

During the cycling of refrigeration, thermal entropy is absorbed by the working material or refrigerant from the cooling load, which is in thermal contact with the load, i.e. isothermal entropy change $\Delta S$. Then, the material is isolated from the load, whereas the temperature is increased due to the application of an external field, i.e. an adiabatic temperature change $\Delta T$ is present. Meanwhile,

the material is in thermal contact with a heat sink, to which the entropy absorbed from the cooling load is ejected. Because the working material is isolated from the heat sink, the temperature is decreased to that of the cooling load, as the field is reduced and the process is repeated. As a result, the isothermal electrical entropy change $\Delta S$ and the adiabatic temperature change $\Delta T$ are the two key parameters that are used to characterize the ECE.

The performances of different refrigerants can be characterized by using a parameter known as refrigerant capacity (RC), which is expressed as $\Delta S_c \Delta T_{hc}$ [33]. Here, $\Delta S_c$ is the isothermal entropy change at $T_c$ and $\Delta T_{hc} = T_h - T_c$ is the temperature span of the refrigeration cycle, where $T_h$ and $T_c$ are the hot end and cold end temperatures, respectively. Figure 1.3 shows a schematic diagram demonstrating the refrigeration cycle [21]. For the ECE of a dielectric material to be used as the refrigerant, $\Delta T_{hc}$ and $\Delta S_c$ can vary as a function of electric field. Also, the largest value of $\Delta S_c \Delta T_{hc}$ at a selected operation temperature should be used as a measure to characterize the performance of a refrigerant. Phenomenological theory has been used widely in the study of ferroelectric materials, which is also useful in guiding the development of ferroelectrics to achieve a large ECE.

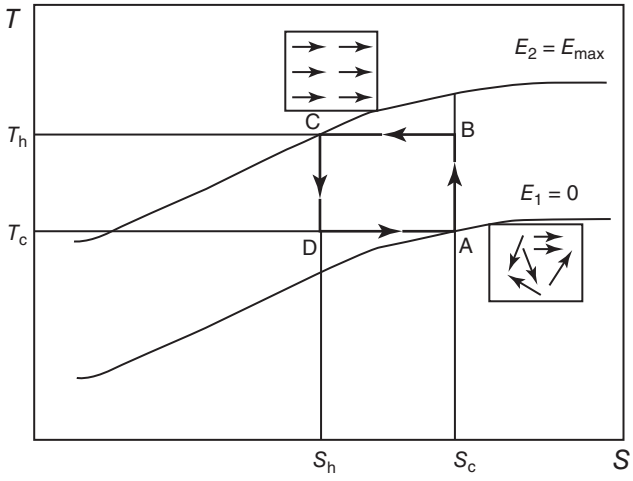


**Figure 1.3** Schematic diagram of a potential thermodynamic refrigeration cycle based on EC effect that is similar to a Carnot cycle. From the path of (A)–(B) and then (B)–(C), an applied electric field is raised from $E_1$ to $E_2$, which induces a polar-ordered phase. From (A) to (B), the EC effect material experiences an adiabatic temperature change $\Delta T_{hc}$ from $T_c$ to $T_h$, and then from (B) to (C) it ejects heat (entropy) to the heat sink at $T_h$ while the material entropy is reduced from $S_c$ to $S_h$ (isothermal entropy change $\Delta S$). From the path of (C) to (D) and then (D) to (A), the applied electric field is reduced from $E_2$ to $E_1$ and the EC effect material loses polar ordering. Accompanying this, the EC effect material experiences a decrease in temperature from $T_h$ to $T_c$ from (C) to (D) (adiabatic temperature change) and then absorbs heat (entropy) from the cold load (isothermal entropy change). Because the EC effect materials of interest are insulators, the above electric field (refrigeration) cycle has the potential of very low electric loss, and consequently, the cooling devices based on the EC effect have the potential to reach very high efficiency. *Source:* Lu and Zhang 2009 [21]. Reproduced with permission of John Wiley & Sons.

According to the general form of the Gibbs free energy related to polarization as discussed earlier, the entropy and adiabatic temperature changes are given by [32]

$$\Delta S = -\frac{1}{2}\beta D^2 \tag{1.97}$$

$$\Delta T = -\frac{1}{2c_E}\beta T D^2 \tag{1.98}$$

As expected, as the material develops a polar phase its entropy will decrease, and Eq. (1.97) indicates that this entropy change is proportional to the square of the electric displacement change. Furthermore, Eq. (1.97) also indicates that a dielectric material with a large $b$ will exhibit a large $\Delta S$.

It is expected that the change in entropy at an external electric field can be treated as the alignment of dipoles. Therefore, below a critical point, the degree of alignment is proportional to the electrical field. However, once approaching the critical point, all the dipoles are aligned, so that saturation is reached. In this case, there will be no change in entropy as the electric field is further increased [22]. That critical point corresponds to a physical upper limit for a given material, which is accompanied by an EC temperature change, known as the saturated EC temperature change, $\Delta T_{\text{sat}}$. According to thermodynamic and statistical mechanics, $\Delta T_{\text{sat}}$ can be expressed as [34]

$$\Delta T_{\text{sat}} = \frac{kT \ln \Omega}{3\varepsilon_0 \Theta C_E} \tag{1.99}$$

where $\Omega$ is the number of discrete equilibrium orientations of dipolar entities, $C_E$ is the volume specific heat, $\Theta$ is the Curie constant, $k$ is the Plank constant, and $T$ is the absolute temperature. However, most of the experimental values of EC are lower than the calculated $\Delta T_{\text{sat}}$, while much higher values have been observed in some oxide ferroelectric thin films. This observation has not been well clarified, which could be attributed to either the inaccuracy of the experimental measurement or prematurity of the theoretical estimation.

When comparing a 1-μm thin film and a 1-mm-thick ceramic sheet, with $\Delta T$ of 10 and 1 K, respectively, the cooling capacity of the ceramic sample is 100 times that of the thin film. Therefore, from a practical application point of view, thin films cannot be used for mid- and large-scale cooling applications. In this regard, it is still necessary to explore ferroelectric ceramics or single crystals for large-scale EC applications. Additionally, high dielectric strength is another important requirement to achieve high-performance ECEs. This is the main reason why relatively high EC temperature changes have been observed in ferroelectric thin films, because the dielectric strength is inversely proportional to thickness of the samples. The dependence of dielectric strength ($E_{\text{b}}$) on the thickness of a material has the following relationship [35]:

$$E_{\text{b}} \propto t^{-n} \tag{1.100}$$

where $t$ is the thickness and $n$ is a fitting parameter that is closely related to microstructure and charge transfer of the material. Generally, in an $E_{\text{b}} - t$ curve, the dielectric strength abruptly decreases with increasing thickness initially

and the decreasing rate slows down, which is attributed to the change in the breakdown mechanism [36]. For instance, electron ionization avalanche mechanism is responsible for the breakdown for thin films, while electromechanical breakdown becomes dominant as the thickness of the films is increased [37]. It is expected that if the microstructural features inside the bulk ceramics could be eliminated, high dielectric strength and thus high EC temperature changes could be achieved. Therefore, increasing the breakdown strength of bulk ceramics should be a challenge in developing EC materials for practical applications.

## 1.5 Ferroelectric Photovoltaic Solar Energy Harvesting

Recently, the coupling of polarization with optical properties in ferroelectric materials with small bandgaps has drawn much attention, due to the potential photovoltaic effects [38–40]. Because of their non-centrosymmetric crystal structure, ferroelectric materials were found to exhibit an unconventional photovoltaic behavior, which is known as bulk photovoltaic effect (BPVE) [41]. A strikingly high power conversion efficiency (PCE) of 8.1% has been achieved in multilayered $Bi_2FeCrO_6$ thin film solar cells [42]. Because Si-based solar cells work on the principle of p–n junction, they are governed by the Shockley–Queisser limit [43]. In contrast, the BPVE does not encounter such a problem. Besides the BPVE, there are other factors that can be considered when using ferroelectric-based photovoltaics. For instance, according to a semiconductor-based model, with a charge distribution in the ferroelectric, which could be polarization surface charges, Schottky-induced space charges, and screening charges in the electrodes, a high photovoltaic efficiency of 19.5% has been predicted in thin films with a thickness of 1.2 nm [44].

Another important parameter is called fill factor (FF), which is defined as the maximum power in the current–voltage curve that is divided by the product of the short-circuit photovoltaic current and the open-circuit photovoltage. As compared with the conventional semiconductor solar cells that have FF of up to 80%, the values of FF of photo-ferroelectrics are only in the range of 10–30% [11, 45]. Such low FF values have been ascribed to the resistive losses of the devices, due to the poor contact of electrodes and the presence of defects in the materials. Other intrinsic resistances could be from grain boundaries and even the domain walls. Therefore, there is still plenty of room to improve the performances of ferroelectric photovoltaic materials.

The photovoltaic effect of ferroelectric materials was first observed in $BaTiO_3$, with a steady photovoltaic current, together with a weak pyroelectric current above the Curie temperature [46]. It was ascribed to the presence of a surface charged layer, which was trapped as the material was heated above the Curie temperature. Following that, the effect was quantitatively analyzed, eventually leading to the establishment of models for the photovoltaic effect of ferroelectrics – for example, a steady photovoltaic current, i.e. electrical current flowing in a short-circuited sample under illumination in $BaTiO_3$ [47] and $Fe^{2+}$-doped $LiNbO_3$ [48]. The photovoltaic current in $Fe^{2+}$-doped $LiNbO_3$ was

attributed to the asymmetric scattering of the excited electrons related to the Fe impurities [49]. Because the Fe impurities in $LiNbO_3$ crystal occupied the non-centrosymmetric sites, the potential barriers for electrons were different in different directions. For instance, if one direction is more favorable than others, there will be more electrons statistically in this direction with a definite momentum vector, thus leading to the presence a nonvanishing photovoltaic current. As a consequence, there are more photoexcited electrons, which in turn increase the imbalance and thus the photovoltaic current.

Besides the asymmetric scattering of free electrons, Franck–Condon relaxation of excited ions is another fact that could be responsible for the generation of the photovoltaic current. According to the asymmetric scattering model, the short-circuit photovoltaic current ($J_{sc}$) is proportional to the intensity ($I$) of the monochromatic incident light, which is given by [49, 50]

$$J_{SC} = \kappa_1 \alpha I \tag{1.101}$$

where $\alpha$ is the absorption coefficient and $\kappa_1$ is a constant that is dependent on factors including the characteristics and concentration of the impurity center, mean free path of the excited electron, and the energy level of the incident photons.

Although this model was further elaborated by using a fully quantum calculation to account for the scattering of excited electrons through the introduction of an asymmetric quantum well [51], it could not be used to explain the sinusoidal variation in the photovoltaic current observed in the Fe:$LiNbO_3$ crystal, as the linear polarization of the incident light was rotated [41]. To explain this observation, a second-order optical response has to be employed to describe the BPVE by using a third-rank tensor [52–54]. As a non-centrosymmetric material is irradiated with an incident electromagnetic plane wave $E_{inc}$, with frequency $\omega$, wavevector $\boldsymbol{k}$, unit polarization vector $\boldsymbol{e}$, and amplitude $E_0$, i.e.

$$E_{inc} = eE_0 e^{i(k,r-\omega t)} + e^* E_0 e^{-i(k,r-\omega t)} \tag{1.102}$$

the current density $j$ is usually expressed as a Taylor expansion in terms of both the applied electric field $E_{ext}$ and the incident light electric field having intensity $I = E^*_{inc} \cdot E_{inc}$, as follows [55]:

$$j_i = \sigma_{ij} E_j^{ext} + \sigma_{ijl} E_j^{ext} E_l^{ext} + \sigma_{ijlm} E_j^{ext} e_l e_m^* I + \chi_{ijlm} q_j e_l e_m^* I + \beta_{ijl} e_j e_l^* I + \cdots \tag{1.103}$$

The first term is known as the basic Ohm's response to an external applied electric field, which is given by the conductivity tensor $\sigma_{ij}$. The second one is the nonlinear correction to Ohm's law, corresponding to the tensor $\sigma_{ijl}$. The third term stands for the photoconductivity effect, corresponding to the photoconductivity tensor $\sigma_{ijlm}$. The fourth term is called the light entrainment effect, which generally can be neglected. The last term describes the BPVE. Since the current density is a real quantity, while the photovoltaic tensor $\beta_{ijl}$ is a complex value, the latter should be separated into real and imaginary parts. The real part $\beta^L$ describes the linear photovoltaic effect (LPVE) caused by the linearly polarized incident light, whereas the imaginary part $\beta^C$ represents the circular photovoltaic effect

(CPVE) due to the circularly polarized incident light. The short-circuit current, $j_{sc}$, due to the BPVE, is given by

$$j_i^{SC} = \beta_{ijl}^{L} e_j e_l^* I + i\beta_{il}^{C}[e \times e^*]_l I \tag{1.104}$$

Because the BPVE is expressed as a third-rank tensor, it is only observed in materials without inversion center. Therefore, materials belonging to the 21 piezoelectric crystal classes, as stated earlier, could potentially have BPVE effect, which has been confirmed by experimental measurement results of various materials.

The BPVE photovoltaic current can be expressed in terms of microscopic quantities, given by [52]

$$j_{SC} = e\alpha(\omega)\left(\frac{I}{\hbar\omega}\right)\xi(\omega) \tag{1.105}$$

where $e$ is the elementary charge of the electron, $\omega$ is the incident light pulsation, and $\xi(\omega)$ is the typical mean free path that the coherent carriers traveled in the favored direction, which is a measure of the distance that the non-thermalized or ballistic carriers would travel in a given anisotropy direction. In addition, a shift current theory was developed to describe the BPVE of ferroelectric materials [56]. Accordingly, the BPVE tensor is expressed as the product of two items: (i) transition intensity that is proportional to the absorption between the $i$th and $j$th directions of incident light, $I_{ij}$, and (ii) shift vector in the $l$th direction, $R_l$, i.e.

$$\beta_{ijl}^{L}(\omega) = e\sum_{n',n''}\int dk I_{ij}(n', n'', k, \omega)R_l(n', n'', k) \tag{1.106}$$

In this case, the summation over $n'$ and $n''$ is over the different bands, whereas that over $k$ is over the whole Brillouin zone. Equation (1.105) indicates that the necessary asymmetry in $k$-space could be developed in different ways, in order to achieve high photovoltaic currents. Meanwhile, the summation over the Brillouin zone can be asymmetric, especially when the degrees of freedom of spin are involved, because of the breaking of symmetry of time inversion. Furthermore, the shift vector could be anisotropic in $k$-space, so that the scattering of the states associated with an asymmetric potential well would be different with different wavevectors.

The significant progress of photovoltaic effect in ferroelectrics was the observation of the switchable diode behavior in $BiFeO_3$ (BFO) single crystals [38]. At the same time, another important discovery involves the periodic array of 71° domain walls in BFO thin films, as shown in Figure 1.4 [57]. As the thin films samples were illuminated with a white light of 28.5 mW cm$^{-2}$, an above-bandgap open-circuit photovoltage of 16 V and an in-plane photovoltaic current of 120 μA cm$^{-2}$ were obtained. Furthermore, the photovoltage had a linear relation to the spacing of the electrode, which implied that it increased with increasing number of domain walls. At the same time, it was found that single domain BFO samples exhibited no photovoltaic effect. Moreover, photovoltaic effect was only observed as the electrodes were parallel to the domain walls (PLDW), whereas there was no photovoltaic effect if the electrodes were perpendicular to the domain walls (PPDW).

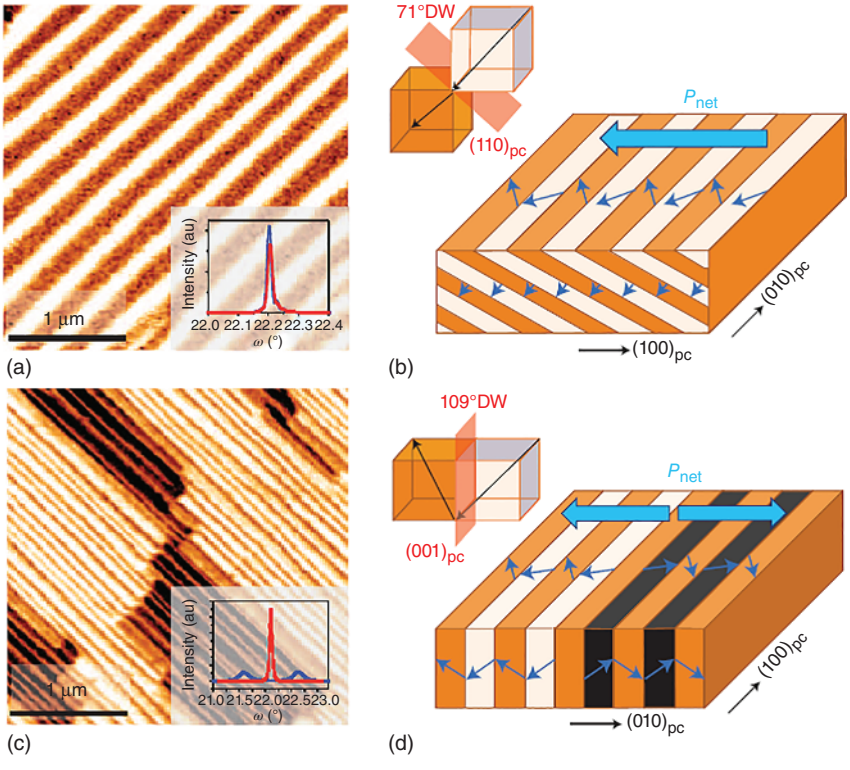


**Figure 1.4** (a) Piezoresponse force microscopy (PFM) image of the ordered arrays of 71° domain walls. *Inset:* Corresponding X-ray rocking curves, along two orthogonal crystal axes. (b) Schematic diagram of the 71° domain wall arrays. The arrows indicate the different components of polarization (in-plane and out-of-plane), as well as the net polarization direction (large arrow) in the samples. Samples are found to have net polarization in the plane of the film. (c) PFM image of the ordered arrays of 109° domain walls. Inset shows the corresponding X-ray rocking curves, along two orthogonal crystal axes. (d) Schematic diagram of the 109° domain wall arrays. *Source:* Yang et al. 2010 [57]. Reproduced with permission of Springer Nature.

The domain wall photovoltaic effect (DWPVE) has been explained by considering the domain wall potential. Generally, there is a drop in potential across a domain wall in $BiFeO_3$, which is related to the rigid rotation of the polarization [58]. The level of such a drop is in the order of 180° DWs > 109° DWs > 71° DWs [59]. Accordingly, it was assumed that the potential drop could build up a high electric field in the DWs, so that electrons would be effectively separated from holes [60]. Meanwhile, recombination could also occur in the domains, since the internal electric field might not be sufficiently strong. As a result, carriers would be accumulated on different sides of the DWs, thus making them behave in a manner similar to a p–n junction.

More recently, the DWPVE model encountered serious challenges. For instance, first-principle calculations indicated that the bandgap variations predicted at the walls of BFO could not be generated [61]. Also, the assumption in

the model that there is a recombination in the domains, due to the insufficiently strong electric field to dissociate the photogenerated electron–hole pairs, has not been confirmed experimentally. In an attempt to probe the local photoelectric effect of a single crystal of $BiFeO_3$ by using atomic force microscopy (AFM), the $I–V$ curves revealed no significant difference in responses between domains and domain walls [62]. Instead, the origination of PV effect of ferroelectric materials from BPVE was further confirmed [63].

However, a recent study of photovoltaic, photoconductive, and electrical conductive properties of 109° and 71° DW arrays in BFO, as a function of temperature, has clarified the roles of domain walls [64]. To avoid the effects of asymmetric contacts, symmetric Pt electrodes were employed in the study, where a photovoltage of as high as 7 V was observed for the 71° DWs with PPDW and PLDW configurations. Meanwhile, for 109° DWs, a photovoltage of 5.4 V was achieved with the PLDW configuration, whereas the PPDW configuration had no PV effect. Additionally, in all cases, the open-circuit voltage was decreased exponentially with increasing temperature, while the electrical conductivity and the photoconductivity were exponentially increased. If the photovoltaic current is assumed to be constant, the photovoltage is related to both the electrical conductivity $\sigma$ and the photoconductivity $\sigma_{ph}$, which is given by

$$V_{\propto} = \frac{L}{\sigma + \sigma_{ph}} J_{SC} \tag{1.107}$$

where $L$ is the spacing between the electrodes. It can be used to describe the exponential decrease in the photovoltage with temperature. The domain walls seemed only to modulate the global conductivity of the materials. In the PLDW configuration, the domain walls increased the resistance by adding an additional resistance to the bulk one, whereas in the PPDW configuration, the domain walls behaved as a shunt, because the domain walls of $BiFeO_3$ have higher electrical conductivity than the bulk [65–67]. It was experimentally demonstrated that the photovoltaic current was varied as the direction of polarization of the light was rotated [64], which is in good agreement with the tensor model of the BPVE, as mentioned above [54]. In summary, the photovoltaic effect observed in ferroelectric materials is intrinsic and has a tensorial nature, which is a bulk property. Besides the contribution of domain walls, the photovoltaic effect in ferroelectric materials can also be tailored by altering external parameters, such as electric field, configuration of electrodes, and creation of defects.

## 1.6 Concluding Remarks

Ferroelectric materials form a special group of materials with various unique properties that can be used for a wide range of applications in different areas. With the recent global research focus on energy generation and harvesting, ferroelectric materials have drawn renewed attention and interest worldwide, because of their potential energy related applications. Piezoelectric properties of ferroelectric materials enable the harvesting of waste mechanical energy in various ways, with the key issues laying on design of devices based on the principles to

have higher efficiencies. Various devices have been developed to harvest different types of mechanical energy. More work is needed to further improve their performances. Pyroelectric effect has been employed to harvest waste thermal energy, but with similar problems as the piezoelectric ones. Developing new materials with higher pyroelectric coefficients seems to be a difficult task, while there is still plenty of room to improve the thermal energy harvesting efficiency through device design. The study of ECE of ferroelectric materials should be focused on the development of bulk ceramics with higher dielectric breakdown strengths, whereas their photovoltaic effects still have unsolved issues.

## References


1 Lines, M.E. (1979). *Glass AM. Principles and Applications of Ferroelectrics and Related Materials*. Oxford: Clarendon Press.

2 Valasek, J. (1921). Piezo-electric and allied phenomena in Rochelle salt. *Physical Review* 17: 475–481.

3 Valasek, J. (1927). Note on the piezo-electric effect in Rochelle salt crystals. *Science* 65: 235–236.

4 Haertling, G.H. (1999). Ferroelectric ceramics: history and technology. *Journal of the American Ceramic Society* 82: 797–818.

5 Damjanovic, D. (1998). Ferroelectric, dielectric and piezoelectric properties of ferroelectric thin films and ceramics. *Reports on Progress in Physics* 61: 1267–1324.

6 Chandra, P. and Littlewood, P.B. (2007). A Landau primer for ferroelectrics. In: *Physics of Ferroelectrics: A Modern Perspective* (ed. K.M. Rabe, C.H. Ahn and J.M. Triscone), 69–115. Springer.

7 Randall, C.A., Kim, N., Kucera, J.P. et al. (1998). Intrinsic and extrinsic size effects in fine-grained morphotropic-phase-boundary lead zirconate titanate ceramics. *Journal of the American Ceramic Society* 81: 677–688.

8 Rodel, J., Jo, W., Seifert, K.T.P. et al. (2009). Perspective on the development of lead-free piezoceramics. *Journal of the American Ceramic Society* 92: 1153–1177.

9 Cook-Chennault, K.A., Thambi, N., and Sastry, A.M. (2008). Powering MEMS portable devices – a review of non-regenerative and regenerative power supply systems with special emphasis on piezoelectric energy harvesting systems. *Smart Materials and Structures* 17: 043001.

10 Beeby, S.P., Tudor, M.J., and White, N.M. (2006). Energy harvesting vibration sources for microsystems applications. *Measurement Science and Technology* 17: R175–R195.

11 Chakrabartty, J., Nechache, R., Li, S. et al. (2014). Photovoltaic properties of multiferroic $BiFeO_3/BiCrO_3$ heterostructures. *Journal of the American Ceramic Society* 97: 1837–1840.

12 Whatmore, R.W. (1986). Pyroelectric devices and materials. *Reports on Progress in Physics* 49: 1335–1386.

13 Bowen, C.R., Taylor, J., LeBoulbar, E. et al. (2014). Pyroelectric materials and devices for energy harvesting applications. *Energy & Environmental Science* 7: 3836–3856.

14 Lang, S.B. (2004). A 2400 year history of pyroelectricity: from Ancient Greece to exploration of the solar system. *British Ceramic Transactions* 103: 65–70.

15 Lang, S.B. (2005). Pyroelectricity: from ancient curiosity to modern imaging tool. *Physics Today* 58: 31–36.

16 Liu, S.T. and Long, D. (1978). Pyroelectric detectors and materials. *Proceedings of the IEEE* 66: 14–26.

17 Kosorotov, V.F., Kremenchugskij, L.S., Levash, L.V., and Shchedrina, L.V. (1986). Tertiary pyroelectric effect in lithium niobate and lithium tantalate crystals. *Ferroelectrics* 70: 27–37.

18 Poprawski, R. (1981). Investigation of phase-transitions in $NH_4HSeO_4$ crystals by pyroelectric method. *Ferroelectrics* 33: 23–24.

19 Devonshire, A.F. (1954). Theory of ferroelectrics. *Advances in Physics* 3: 85–130.

20 Zeyfang, R.R., Sehr, W.H., and Kiehl, K.V. (1976). Enhanced pyroelectric properties at a FE-FE phase transition. *Ferroelectrics* 11: 355–358.

21 Lu, S.G. and Zhang, Q.M. (2009). Electrocaloric materials for solid-state refrigeration. *Advanced Materials* 21: 1983–1987.

22 Valant, M. (2012). Electrocaloric materials for future solid-state refrigeration technologies. *Progress in Materials Science* 57: 980–1009.

23 Li, X.Y., Lu, S.G., Chen, X.Z. et al. (2013). Pyroelectric and electrocaloric materials. *Journal of Materials Chemistry C* 1: 23–37.

24 Scott, J.F. (2011). Electrocaloric materials. *Annual Review of Materials Research* 41: 229–240.

25 Lang, S.B. (1976). Cryogenic refrigeration utilizing the electrocaloric effect in pyroelectric lithium sulfonate monohydrate. *Ferroelectrics* 519–523.

26 Kobeko, P.P. and Kurchatov, I.V. (1930). Dielectric characteristics of Seignette's salts. *Zeitschrift fuer Physik* 66: 192–205.

27 Thacher, P.D. (1968). Electrocaloric effects in some ferroelectric and antiferroelectric $Pb(Zr,Ti)O_3$ compounds. *Journal of Applied Physics* 39: 1996–2002.

28 Radebaugh, R., Lawless, W.N., Siegwarth, J.D., and Morrow, A.J. (1979). Feasibility of electrocaloric refrigeration for the 4-15 K temperature range. *Cryogenics* 19: 187–208.

29 Shebanovs, L., Borman, K., Lawless, W.N., and Kalvane, A. (2002). Electrocaloric effect in some perovskite ferroelectric ceramics and multilayer capacitors. *Ferroelectrics* 273: 2515–2520.

30 Mischenko, A.S., Zhang, Q., Scott, J.F. et al. (2006). Giant electrocaloric effect in thin-film $PbZr_{0.95}Ti_{0.05}O_3$. *Science* 311: 1270–1271.

31 Neese, B., Chu, B.J., Lu, S.G. et al. (2008). Large electrocaloric effect in ferroelectric polymers near room temperature. *Science* 321: 821–823.

32 Lines, M.E. and Glass, A.M. (1977). *Principles and Applications of Ferroelectrics and Related Materials*. Oxford: Clarendon Press.

33 Wood, M.E. and Potter, W.H. (1985). General analysis of magnetic refrigeration and its optimization using a new concept – maximization of refrigerant capacity. *Cryogenics* 25: 667–683.

34 Pirc, R., Kutnjak, Z., Blinc, R., and Zhang, Q.M. (2011). Upper bounds on the electrocaloric effect in polar solids. *Applied Physics Letters* 98: 021909.

35 Forlani, F. and Minnaja, N. (1964). Thickness influence in breakdown phenomena of thin dielectric films. *Physica Status Solidi* 4: 311–324.

36 Kim, H.K. and Shi, F.G. (2001). Thickness dependent dielectric strength of a low-permittivity dielectric film. *IEEE Transactions on Dielectrics and Electrical Insulation* 8: 248–252.

37 Agarwal, V.K. and Srivastava, V.K. (1971). Thickness dependence of breakdown field in thin films. *Thin Solid Films* 8: 377–381.

38 Choi, T., Lee, S., Choi, Y.J. et al. (2009). Switchable ferroelectric diode and photovoltaic effect in $BiFeO_3$. *Science* 324: 63–66.

39 Guo, Y.P., Guo, B., Dong, W. et al. (2013). Evidence for oxygen vacancy or ferroelectric polarization induced switchable diode and photovoltaic effects in $BiFeO_3$ based thin films. *Nanotechnology* 24.

40 Paillard, C., Bai, X.F., Infante, I.C. et al. (2016). Photovoltaics with ferroelectrics: current status and beyond. *Advanced Materials* 28: 5153–5168.

41 Barsukova, M.L., Karimov, B.K., Kuznetsov, V.A. et al. (1980). Photo-voltaic effect in $Bi_{12}TiO_{20}$ piezoelectrics. *Fizika Tverdogo Tela* 22: 2870–2871.

42 Nechache, R., Harnagea, C., Li, S. et al. (2015). Bandgap tuning of multiferroic oxide solar cells. *Nature Photonics* 9: 61–67.

43 Shockley, W. and Queisser, H.J. (1961). Detailed balance limit of efficiency of *p–n* junction solar cells. *Journal of Applied Physics* 32: 510–519.

44 Qin, M., Yao, K., and Liang, Y.C. (2009). Photovoltaic mechanisms in ferroelectric thin films with the effects of the electrodes and interfaces. *Applied Physics Letters* 95: 022912.

45 Nechache, R., Harnagea, C., Licoccia, S. et al. (2011). Photovoltaic properties of $Bi_2FeCrO_6$ epitaxial thin films. *Applied Physics Letters* 98: 202902.

46 Chynoweth, A.G. (1956). Surface space-charge layers in barium titanate. *Physical Review* 102: 705–714.

47 Fridkin, V.M., Volk, T.R., Grekov, A.A., and Kosonogov, N.A. (1972). Photodomain effect in $BaTiO_3$. *Ferroelectrics* 4: 169–175.

48 Glass, A.M., Linde, D.V.D., and Negran, T.J. (1974). High-voltage bulk photovaltaic effect and the photorefractive process in $LiNbO_3$. *Applied Physics Letters* 25: 233–235.

49 Glass, A.M., Von der Linde, D., Auston, D.H., and Negran, T.J. (1975). Excited state polarization, bulk photovoltaic effect, and the photorefractive effect in electrically polarized media. *Journal of Electronic Materials* 4: 915–943.

50 Chanussot, G. and Glass, A.M. (1976). A bulk photovoltaic effect due to electron-phonon coupling in polar crystals. *Physics Letters A* 59: 405–407.

51 Von Baltz, R. and Kraut, W. (1978). A model calculation to explain the existence of bulk photocurrents in ferroelectrics. *Solid State Communications* 26: 961–963.

52 Kraut, W. and Von Baltz, R. (1979). Anomalous bulk photovoltaic effect in ferroelectrics: a quadratic response theory. *Physical Review B: Condensed Matter and Materials Physics* 19: 1548–1554.

53 Von Baltz, R. and Kraut, W. (1981). Theory of the bulk photovoltaic effect in pure crystals. *Physical Review B: Condensed Matter and Materials Physics* 23: 5590–5596.

54 Fridkin, V.M. (2001). Bulk photovoltaic effect in noncentrosymmetric crystals. *Crystallography Reports* 46: 654–658.

55 Sturman, B.I. and Fridkin, V.M. (1992). *The Photovoltaic and Photorefractive Effects in Noncentrosymmetric Materials*. Gordon and Breach Science Publishers.

56 Young, S.M. and Rappe, A.M. (2012). First principles calculation of the shift current photovoltaic effect in ferroelectrics. *Physical Review Letters* 109: 116601.

57 Yang, S.Y., Seidel, J., Byrnes, S.J. et al. (2010). Above-bandgap voltages from ferroelectric photovoltaic devices. *Nature Nanotechnology* 5: 143–147.

58 Lubk, A., Gemming, S., and Spaldin, N.A. (2009). First-principles study of ferroelectric domain walls in multiferroic bismuth ferrite. *Physical Review B* 80: 104110.

59 Seidel, J., Yang, S.Y., Alarcon-Llado, E. et al. (2012). Nanoscale probing of high photovoltages at 109° domain walls. *Ferroelectrics* 433: 123–126.

60 Seidel, J., Fu, D.Y., Yang, S.Y. et al. (2011). Efficient photovoltaic current generation at ferroelectric domain walls. *Physical Review Letters* 107: 126805.

61 Dieguez, O., Aguado-Puente, P., Junquera, J., and Iniguez, J. (2013). Domain walls in a perovskite oxide with two primary structural order parameters: first-principles study of $BiFeO_3$. *Physical Review B* 87: 024102.

62 Alexe, M. and Hesse, D. (2011). Tip-enhanced photovoltaic effects in bismuth ferrite. *Nature Communications* 2: 256.

63 Ji, W., Yao, K., and Liang, Y.C. (2011). Evidence of bulk photovoltaic effect and large tensor coefficient in ferroelectric $BiFeO_3$ thin films. *Physical Review B* 84: 094115.

64 Bhatnagar, A., Chaudhuri, A.R., Kim, Y.H. et al. (2013). Role of domain walls in the abnormal photovoltaic effect in $BiFeO_3$. *Nature Communications* 4: 2835.

65 Seidel, J., Martin, L.W., He, Q. et al. (2009). Conduction at domain walls in oxide multiferroics. *Nature Materials* 8: 229–234.

66 Farokhipoor, S. and Noheda, B. (2011). Conduction through 71° domain walls in $BiFeO_3$ thin films. *Physical Review Letters* 107: 127601.

67 Seidel, J., Singh-Bhalla, G., He, Q. et al. (2013). Domain wall functionality in $BiFeO_3$. *Phase Transitions* 86: 53–66.